THE JOURNAL OF PHYSICAL CHEMISTRY Letters

pubs.acs.org/JPCL Letter

Bosonic Charge Carriers in Necklace-like Graphene Nanoribbons

Marcelo L. Pereira Júnior, Geraldo M. e Silva, and Luiz A. Ribeiro Junior*

Cite This: J. Phys. Chem. Lett. 2020, 11, 5538−5543

Read Online

ACCESS | Metrics & More | Article Recommendations

ABSTRACT: Motivated by the success of graphene in flat optoelectronics, several carbon allotropes have recently been proposed. One of these allotropes, graphene nanoribbons (GNRs) with a singular "necklace-like" atomic structure, was recently synthesized through a bottom-up chemical approach. The absorption spectrum exhibited a band gap of 1.4 eV for this novel GNR geometry. Guided by its exciting electronic and structural properties, investigations should be performed to outline the major features of this material focused on expanding organic-based energy conversion and storage applications. In particular, the formation and dynamics of charge carriers are crucial in defining the material's performance. Here we describe the formation and transport of charge carriers in necklace-like graphene nanoribbons (NGNRs). A 2D tight-binding Hamiltonian endowed with lattice relaxation effects constitutes the basis of the theoretical approach employed to examine the carrier formation and dynamics in these lattices. Results demonstrate that polarons and effective boson species are spontaneously generated in NGNRs by the addition of holes or electrons to the system. Both types of generated quasiparticles are dynamically stable and can move at surprisingly low electric-field regimes. Remarkably, the formation of effective bosons is a process triggered by a higher density of added charges. The understanding of the carriers' formation and transport in NGNRs can pave the way for their broad usage in producing novel optoelectronic applications, added to the possibility of Bose−Einstein condensate phenomena.

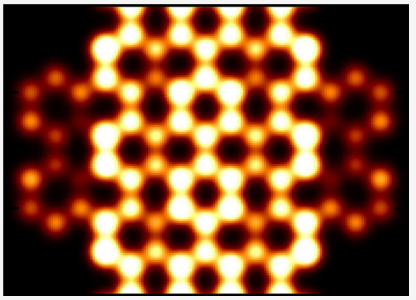

Optoelectronic devices are those that capture, emit, and control light.[1] Nowadays, their organic-based alternatives have been employed to develop a wide range of technological applications, such as field-effect transistors,[2] displays,[3] and photovoltaic cells.[4] Because of their ease of recycling, low production cost, and attractive optical and electronic properties, organic materials are the most promising candidates in replacing conventional inorganic (silicon-based) technology, which can promote advancements in green energy solutions.[5] In early 2000, graphene emerged as an exciting material in developing a novel class of flat optoelectronics.[6,7] However, its null band gap represents a drawback for applications in which semiconducting materials are desirable.

To overcome this obstacle, graphene nanoribbons (GNRs), quasi-1D structures formed from long cuts in graphene sheets, have emerged as interesting solutions because they present a finite band gap, which can vary from 0.2 to 2.5 eV, and preserve most of the interesting structural and electronic properties concerning a graphene sheet.[8−10] Conventional GNRs have two distinct edge endings, namely, armchair (AGNR) and zigzag (ZGNR) graphene nanoribbons, which are directly related to the electronic properties presented by a GNR lattice. ZGNRs have metallic band gaps, and AGNRs, in turn, possess null (or not null) band gaps depending on their width.[8] In this sense, AGNRs are divided into $n = 3p$, $n = 3p + 1$, and $n = 3p + 2$ families, where n is the number of atoms present in the width of the GNR, and p is a positive integer.[8] AGNRs belonging to the $3p + 2$ family have null band gaps.[8] On the contrary, the $n = 3p$ and $n = 3p + 1$ AGNR families have a finite band gap within the previously mentioned range.

In organic materials, the addition of charge may cause the rearrangement of atoms locally (lattice polarization), which yields a cloud of phonons coupled to the extra charge. The mutual electron−lattice interaction leads to the formation of a new quasiparticle, named the polaron, that has a spin $\pm 1/2$ and a charge $\pm e$.[11] Polarons have smaller net mobility and lager effective mass regarding free electrons as a consequence of the electron−phonon coupling mechanism. Two polarons of the same charge and antiparallel spins can merge to form a bipolaron, which is a spinless structure with a charge of $\pm 2e$.[12] Even though it is well accepted that these species are the main species responsible for playing a role in the charge transport in organic materials, the description of the formation and transport of charge carriers in GNR-based materials is still challenging.

Recently, Schwab and coworkers performed the synthesis of a polycyclic aromatic hydrocarbon composed of 84 sp^2-type carbons (C84).[13] This compound was used in the synthesis of

Received: May 14, 2020
Accepted: June 17, 2020
Published: June 17, 2020

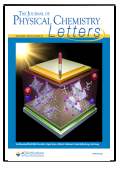

NGNRs by using a bottom-up chemical approach based on the oxidative cyclodehydrogenation of tailor-made polyphenylene precursors.[13] In their study, the absorption spectrum revealed a band gap of ∼1.4 for the novel NGNR structures.[13] Moreover, in the same work, density functional theory (DFT) calculations predicted a band gap of 2.17 for this material.[13] These band-gap values are a piece of evidence that NGNRs can be of great interest for semiconducting-like applications based on low-dimensional systems. In this sense, the charge-transport mechanism (i.e, the formation and dynamics of quasiparticles) in these materials should be understood in detail to promote its wide usage in flat optoelectronics.

Herein the generation and transport of charge carriers in NGNRs lattices are investigated by employing a semiclassical transport approach that considers an external electric field. A 2D tight-binding Hamiltonian endowed with lattice relaxation effects constitutes the basis of our computational protocol. In particular, the formation of novel (boson-like) species of quasiparticles in a graphene-based structure is the main result obtained by the present work. Notably, the results reveal that effective boson species are spontaneously generated in NGNRs by the addition of free electrons or holes to the system. Importantly, the formation of effective bosons is a process triggered by the high density of these particles.

The NGNR is a quasi-1D structure with a minimum/maximum width of 9/15 atoms,[13] as illustrated in Figure 1. It

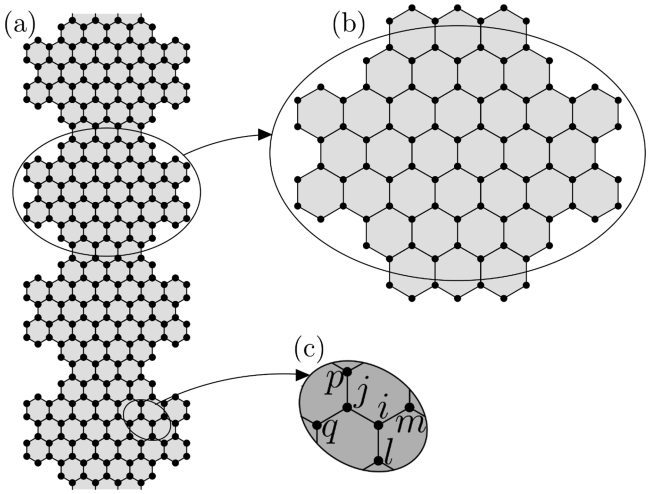

Figure 1. Schematic representation of the atomic structure of a necklace-like graphene nanoribbon: (a) wide view, (b) unit cell, and (c) labeling system.

can be understood as the heterojunction of two $n = 3p$ family nanoribbons, which is known for presenting semiconducting band gaps.[8] The NGNR moiety with the largest width has four lines of carbon atoms, whereas the one with the smallest width has only two atomic lines, as can be seen in Figure 1a.

The NGNR unit cell is presented in Figure 1b. To study the formation and dynamics of quasiparticles in this GNR allotrope, a semiclassical Hamiltonian (based on the Su–Schrieffer–Heeger model[14]) is applied where the π electrons are described by quantum mechanics, within the second quantization formalism, whereas the site displacements are classically treated. The expression of our total model Hamiltonian is given by $H = H_{elec} + H_{latt}$, where the electronic term (H_{elec}) assumes the following form

$$H_{elec} = -\sum_{\langle i,j\rangle,s} (t_{i,j}C_{i,s}^{\dagger}C_{j,s} + t_{i,j}^{*}C_{j,s}^{\dagger}C_{i,s}) \quad (1)$$

where $\langle i, j\rangle$ stands for the indexes of neighboring sites i and j. (See Figure 1c.) $C_{i,s}^{\dagger}$ ($C_{j,s}$) is the annihilation (creation) operator of a π electron in an i (j) site with spin s. Because the variation of the σ-bond lengths is very small in graphene,[15] the electronic transfer integrals can be expanded in the first order. In this way, the hopping integral is written as

$$t_{i,j} = (t_0 - \alpha\eta_{i,j})e^{-i\gamma \mathbf{A}\cdot\hat{\mathbf{r}}_{i,j}} \quad (2)$$

where t_0 is the transfer integral for an undistorted system, $\eta_{i,j}$ denotes the variation in the bond length of two neighboring sites i and j, and α is the electron–phonon coupling parameter that connects the electronic and lattice degrees of freedom.[16] To consider the quasiparticle dynamics, an external electric field, $\mathbf{E}(t)$, was included by employing a time-dependent vector potential, $\mathbf{A}(t)$, using a Peierls substitution for the phase factor of the electronic transfer integral.[15] In this equation, $\gamma \equiv ea/(\hbar c)$, where a is the lattice parameter, e is the absolute value of the electronic charge, and c represents the speed of light. The relationship between the time-dependent electric field and the vector potential is given by $\mathbf{E}(t) = -\frac{1}{c}\frac{d\mathbf{A}(t)}{dt}$. Here the electric field is turned on adiabatically, as described in ref 17.

The second part of our model Hamiltonian (H_{latt}) describes the lattice backbone according to

$$H_{latt} = \frac{1}{2}\sum_{\langle i,j\rangle} K\eta_{i,j}^{2} + \frac{1}{2}\sum_{l}\frac{P_l^2}{M} \quad (3)$$

where the first part describes the σ-bonding energies within the harmonic approximation, where K is the elastic constant. The last part of eq 3 takes into account the kinetic energies of carbon atoms (lattice sites) in the system, with M being the mass of each site and P_l their momenta. The index l runs over all lattice sites. The model parameters employed here are t_0 = 2.7 eV, α = 5.2 eV/Å, K = 21 eV/Å^2, and M = 12 u, which were experimentally[7,15] or theoretically[15,18] reported in the literature and also used in other theoretical works, presenting a good track record.[19−22] By employing this set of parameters, we have obtained a band gap of 1.62 eV through a density of states calculation following the procedure described in ref 23, which is closer to the experimental value than DFT calculations.

To obtain the stationary solution ($P_l = 0$), a self-consistent procedure is used from an initial random set of coordinates $\{\eta_{i,j}\}$. Iteratively, the H_{elec} diagonalization is performed to yield a self-consistent ground-state geometry, which is represented by a converged set of coordinates $\{\eta_{i,j}\}$ and a corresponding set of electronic wave functions $\{\psi_{k,s}\}$.[17] The concomitant self-consistent lattice solution is obtained from the Euler–Lagrange equations

$$\frac{d}{dt}\left(\frac{\partial\langle L\rangle}{\partial\dot{\xi}_l}\right) - \left(\frac{\partial\langle L\rangle}{\partial\xi_l}\right) = 0 \quad (4)$$

where ξ_l are the coordinates of a given site. Importantly, in the static case $\partial\langle L\rangle/\partial\xi_l = 0$. To account the lattice effects, it is necessary to obtain the expected value of the Lagrangian, $\langle\Psi|L|\Psi\rangle$, where $|\Psi\rangle$ is the Slater determinant represented in the second quantization formalism by $|\psi\rangle = a_1^{\dagger}a_2^{\dagger}\ldots a_n^{\dagger}|\rangle$. As

https://dx.doi.org/10.1021/acs.jpclett.0c01489
J. Phys. Chem. Lett. 2020, 11, 5538−5543

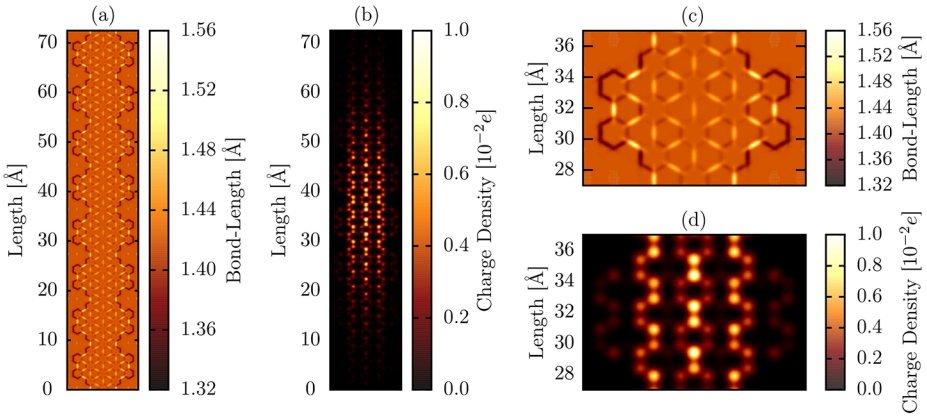

Figure 2. Ground-state solution for a polaron in necklace-like graphene nanoribbons (NGNRs): (a) bond lengths and (b) atomic charge density configurations. (c,d) Zoom-in of the bond lengths and charge-density signatures, respectively, for a region in the lattice that contains a polaronic charge.

$$L = \frac{M}{2}\sum_{l}\dot{\xi}_l^2 - \frac{1}{2}K\sum_{\langle i,j\rangle}\eta_{i,j}^2 + \sum_{\langle i,j\rangle,s}(t_0 - \alpha\eta_{i,j})e^{-i\gamma\mathbf{A}\cdot\hat{\mathbf{r}}_{i,j}}(C_{i,s}^{\dagger}C_{j,s} + C_{j,s}^{\dagger}C_{i,s}) \tag{5}$$

then

$$\langle L\rangle = \frac{M}{2}\sum_{i}\dot{\xi}_i^2 - \frac{1}{2}K\sum_{\langle i,j\rangle}\eta_{i,j}^2 + \sum_{\langle i,j\rangle}(t_0 - \alpha\eta_{i,j})e^{-i\gamma\mathbf{A}\cdot\hat{\mathbf{r}}_{i,j}}(B_{i,j} + B_{i,j}^{*}) \tag{6}$$

with

$$B_{i,j} \equiv \sum_{k,s}{}' \psi_{k,s}^{*}(i,t)\psi_{k,s}(j,t) \tag{7}$$

where the sum is realized only for the occupied states. The last equation is responsible for the connection between the electronic and lattice degrees of freedom. It is important to emphasize that our self-consistent approach can accurately reproduce alternating variations of long and short bonds for the ground-state structure of GNRs.

Starting from the results obtained in the stationary solution, the temporal evolution of the system is governed by the time-dependent Schrödinger's equation (for the electronic degree of freedom) and the Euler−Lagrange equations (when it comes to the lattice degree of freedom), eq 4, that can be rewritten as

$$M\ddot{\eta}_{i,j} = \frac{1}{2}K(\eta_{i,l} + \eta_{m,i} + \eta_{j,p} + \eta_{q,j}) - 2K\eta_{i,j} + \frac{1}{2}\alpha(B_{i,l} + B_{m,i} + B_{j,p} + B_{q,j} - 4B_{i,j} + \text{c.c.})$$

Finally, the time evolution of the wave functions $\{\psi_{k,s}\}$ is stated as follows

$$|\psi_{k,s}(t + \mathrm{d}t)\rangle = \sum_{l}\exp(-i\varepsilon_{l,s}\,\mathrm{d}t/\hbar)|\varphi_{l,s}(t)\rangle\langle\varphi_{l,s}(t)|\psi_{k,s}(t)\rangle \tag{8}$$

where $\{\varepsilon_{l,s}\}$ and $\{|\varphi_{l,s}\rangle\}$ are the eigenvalues and eigenkets of H_{elec} at a given time t, respectively.

To characterize the formation of charge carriers in NGNRs, we have adopted the system with width periodically changing between 9 and 15 atoms, according to Figure 1. As previously mentioned, both GNR moieties belong to the $n = 3p$ family, which presents a semiconducting band gap.[8] Here we assume periodic boundary conditions along the ribbon's length (150 Å) to account for edge effects. The direction of the external electric follows the ribbon's length. A doping process is simulated by removing an electron (or by adding a hole) in an originally neutral NGNR lattice. As a consequence, the lattice is distorted (polarized) and the extra charge is localized in the deformed region, yielding a polaron, as shown in Figure 2. In this figure, panels a and b illustrate the ground-state solution for the bond lengths and the charge density, respectively, for an NGNR lattice in the presence of a polaron. The bond lengths in the central region of the lattice are different from the ones in the edge due to the local deformations imposed by the presence of an extra hole, as illustrated in Figure 2a. Accordingly, the atomic charge is localized in the center of the lattice, being distributed over three rows of carbon rings. The charge concentration diminishes from the center toward the edges and along the ribbon's length. In Figure 2b, it can be observed that the extra charge is distributed along ∼60 Å. In this sense, the probability of finding an electron at the ribbon's outermost part (beyond the minimal width of nine sites) is very small because the lattice is rigid in the edges. These features are in good agreement with experimental observations that have revealed the absence of charge concentration in GNR edges.[24] The combined signatures for bond lengths and atomic charge density, as previously pointed out, characterize the formation of a stable polaron in NGNRs. For the sake of clarity, Figure 2c,d zooms in on the charge-density and bond-length signatures, respectively, for a region in the lattice that contains a part of the polaronic charge.

Figure 3 illustrates the polaron dynamics for different external electric-field regimes, starting from the ground-state solution presented in Figure 2. The electric-field strengths investigated here are 0.2, 0.4, and 0.6 mV/A. After a transient time necessary for the electric field to reach its full strength (40 fs), one can see that the polaron moves linearly as a response to the applied electric field in all of the cases. The saturation velocities range from 0.380 to 0.750 Å/fs. A straightforward calculation, according to ref 25, points to a sound velocity of ∼0.30 Å/fs in NGNRs. In this way, polarons move within the optical regime in NGNRs, even considering low electric-field strengths. Importantly, our results show that polaron velocities in NGNRs are higher than those for narrower GNR lattices (with widths of four, six, and nine carbon atoms[18,22]). This means that the higher degree of charge delocalization in NGNRs, when compared with conventional GNRs (see refs 18 and 21), is responsible for promoting higher velocities.

A surprising result arises when the concentration of additional holes increases in NGNR lattices. Each panel in

https://dx.doi.org/10.1021/acs.jpclett.0c01489
J. Phys. Chem. Lett. 2020, 11, 5538−5543

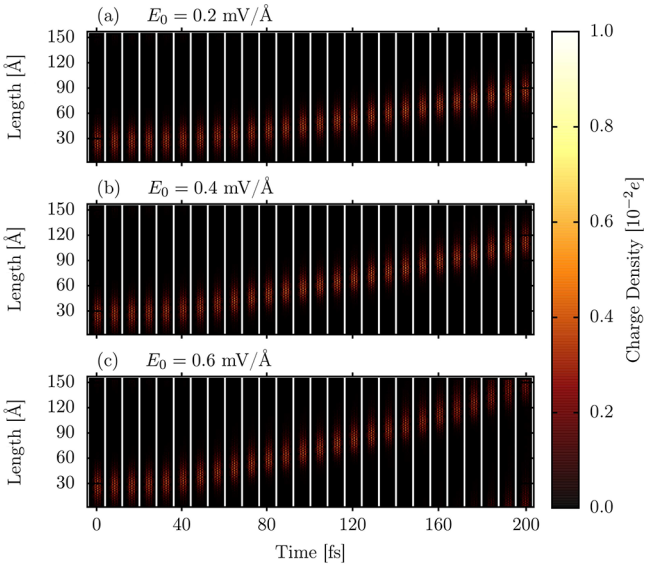

Figure 3. Time evolution of the mean charge-density profile for a necklace-like graphene nanoribbon (NGNR) containing a polaron. The electric-field strengths (E_0) are (a) 0.2, (b) 0.4, and (c) 0.6 mV/Å.

Figure 4 illustrates the ground-state configuration for the charge-density profile considering a different number of holes added to the NGNR lattice, which varies from 1 to 10 extra particles. In Figure 4a–d, one can note that the charge localizes at different places along the lattice, defining the total number of polarons that are formed upon the presence of additional holes. In Figure 4e, we cannot realize a charge-density signature (i.e., multiple charge localization signatures that lie separately from each other) that characterizes the formation of stable polarons. After this critical concentration of free holes, the trend in forming quasiparticles changes abruptly. Figure 4 shows that after the critical number of additional particles (in this case, seven holes), a novel bosonic quasiparticle is generated. The charge-density signature that represents the formation of an effective boson is presented in Figure 4f. One can note a strong light-yellow region in the center of the lattice, representing a higher degree of charge accumulation when contrasted with rest of the system. As previously mentioned, a large concentration of polarons can yield a new carrier that is composed of particles.[16,20] Therefore, among all additional holes, just two of them merge to compose this new species. Consequently, the formed boson is a spinless structure with a charge of 2*e*. It worthwhile to stress that the holes were added by alternating their spin between up and down. In this sense, for an even number of holes, the lattice has the same quantity of particles with up and down spins, whereas for an odd number of holes, the lattice has one additional spin-up particle. Interestingly, when the concentration of particles is increased from eight to nine holes, two bosons are formed (Figure 4g). A similar trend occurs when the number of holes increases to 10, as depicted in Figure 4h. Figure 2c,d zooms in on the bond-length and charge-density signatures, respectively, for a region in the lattice that contains a part of the bosonic charge for the case depicted in Figure 4f. In these figures, one can note that the bond lengths in the center of the lattice present a smaller degree of distortion when contrasted with the polaron case. (See Figure 2.) This result suggests that the novel bosonic species is weakly coupled to the lattice and can move along it as a free carrier. This is actually true, as shown as follows.

Concerning the transport mechanism, the effective bosons present a crucial difference when contrasted with polarons. The charge of this new carrier is coupled to very shallow lattice distortions. In this way, even for considerably small field strengths, the bosonic charge decouples from its local lattice deformations and moves in the NGNR lattice like a free carrier. This behavior differs from the polaron transport mechanism, in which the charge and lattice deformations move as a single composite state. Figure 5 shows the dynamics of an effective boson for the same electric-field strengths considered to analyze the polaron dynamics (Figure 4). The simulations illustrated in Figure 5 consider as a starting point the ground-state configuration for the case presented in Figure 4f. From Figure 5, one can derive the saturation velocities for bosonic quasiparticles in NGNRs, which range from 0.25 to 0.50 Å/fs.

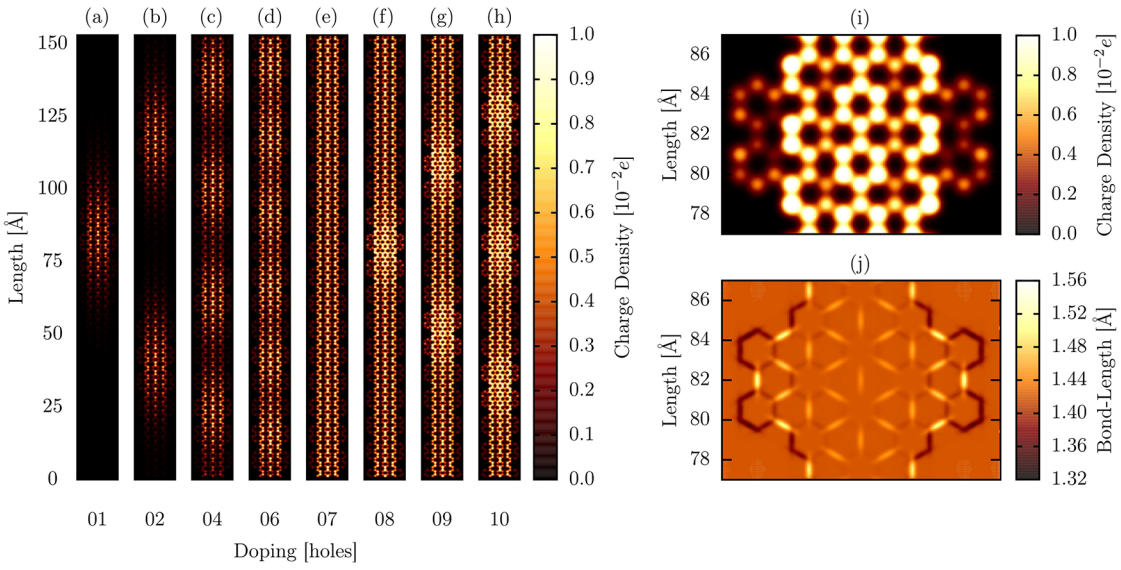

Figure 4. Ground-state solutions for different hole concentrations: (a) 1, (b) 2, (c) 4, (d) 6, (e) 7, (f) 8, (g) 9, and (h) 10. (i,j) Zoom-in of the charge-density and bond-length signatures, respectively, for a region in the lattice that contains part of the bosonic charge.

https://dx.doi.org/10.1021/acs.jpclett.0c01489
J. Phys. Chem. Lett. 2020, 11, 5538–5543

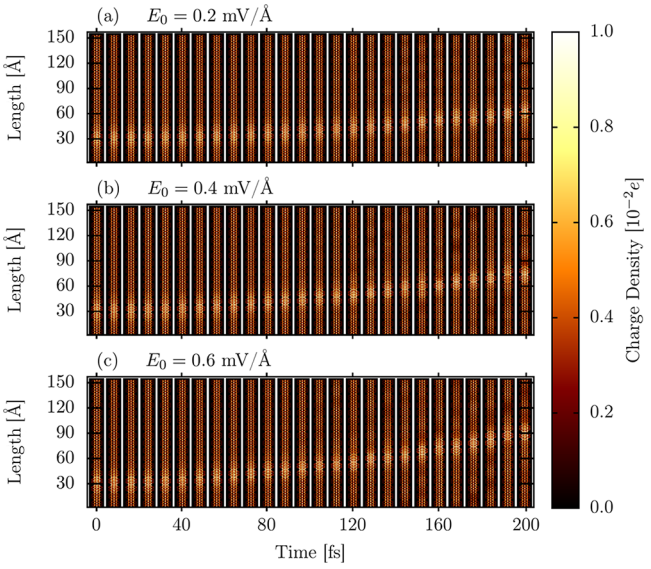

Figure 5. Time evolution of the mean charge-density profile for a necklace-like graphene nanoribbon (NGNR) containing a boson. Three electric-field strengths (E_0) are considered to be: (a) 0.2, (b) 0.4, and (c) 0.6 mV/Å.

It suggests that bosons can move in this material in both acoustic and optical regimes of terminal velocities. Because the bosons formed here are composed of two holes, their effective masses are greater than those of polarons. As a consequence, bosons present lower terminal velocities when compared with polarons for a given electric-field strength, which can be noted by contrasting the time evolution of the atomic charge densities, as presented in Figures 4 (polaron case) and 5 (boson case). Because of the higher effective mass, the boson dynamics in Figure 5 presents a linear motion, as a response to the applied electric field, only after 80 fs.

We finish our discussions by presenting in Figure 6 the time evolution profile of the intragap energy levels of the simulations shown in Figures 3c (polaron case) and 5c (effective boson case). In Figure 6a, one can note the presence of typical polaron steady states within the band gap. These levels remain inside the band gap until the end of the simulation, characterizing that polarons are dynamically stable in NGNR lattices. In contrast, the intragap energy levels related to the effective boson are very close to the conduction and valence bands at the beginning of the simulation, and during the dynamics, they oscillate and return to those bands, as shown in Figure 6b. This signature for the bosonic energy levels is a consequence of the weak coupling between its charge and related lattice distortions. Moreover, their proximity to the conduction and valence bands combined with the small oscillations presented by them denotes the presence of a charge-density wave in the lattice instead of the dynamics of a composite state between an additional charge and the local lattice deformation.

In summary, we have developed a 2D tight-binding Hamiltonian endowed with lattice relaxation effects to study the formation and dynamics of quasiparticles in NGNRs. Here we point to the formation of a novel quasiparticle species (an effective boson) that was not observed in any other graphene allotrope so far. This striking result opens a new channel to understand the charge-transport mechanism in graphene-based systems. Moreover, this new quasiparticle is fully characterized here in terms of its electronic and structural properties. Results have revealed that polarons and effective bosons species are spontaneously generated in NGNRs by adding free holes to the system. Both types of quasiparticles are dynamically stable and can move at surprisingly low electric-field regimes. It is worth mentioning that similar results can be obtained by instead adding electrons. The saturation polaron velocities can range from 0.380 to 0.750 Å/fs, suggesting that polarons in NGNRs move within the optical regime, even at low electric field strengths. Notably, the formation of effective bosons is a process triggered by considering a higher density of holes. After a critical concentration of 0.53%, effective bosonic quasiparticles are generated. It was concluded that the saturation velocities for bosons in NGNRs range from 0.25 to 0.50 Å/fs. In this way, bosons can move in this material in both the acoustic and optical regimes of terminal velocities.

Polarons are formed in both AGNRs and NGNRs. Importantly, bipolarons are not formed in NGNRs. Concerning the transport mechanism, the effective bosons present a crucial difference when contrasted with polarons and bipolarons. The charge of these novel quasiparticles is coupled to very shallow lattice distortions; that is, the bosonic species is weakly coupled to the lattice. In the very first stage of its dynamics, its charge decouples from related distortions moving

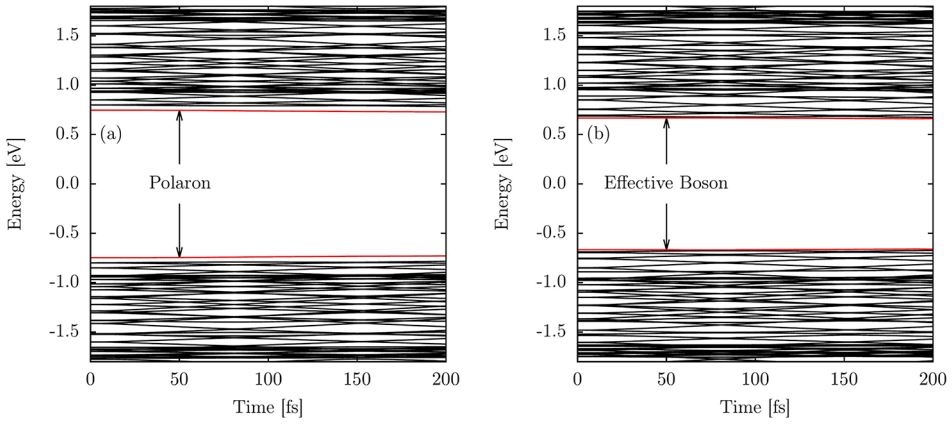

Figure 6. Time evolution of the energy levels for (a) the polaron and (b) an effective boson dynamics considering the electric-field strength of 0.6 mV/Å. The red lines denote the quasiparticles' intragap levels. The cases presented in panels a and b refer to the simulations shown in Figures 3c (polaron case) and 5c (effective boson case), respectively.

https://dx.doi.org/10.1021/acs.jpclett.0c01489
J. Phys. Chem. Lett. 2020, 11, 5538−5543

along the lattice like a free carrier, forming a charge-density wave. This behavior is attributed to the distinct (and very particular) nature of the lattice arrangement presented by NGNRs. When it comes to the dynamics of charge carriers, the terminal velocities of polarons and bipolarons in standard AGNRs can range within the intervals 0.3 to 5.1 Å/fs[26] and 0.05 to 1.30 Å/fs,[23] respectively, depending on the ribbon's width and the strength of the applied electric field. Here, for an electric-field strength of 0.6 mV/Å, we have obtained a terminal polaron velocity of ∼0.6 Å/fs, which is equivalent to the one reported for a standard armchair nanoribbon considering the same electric-field strength.[26] For the novel bosonic species, we have obtained here a terminal velocity of 0.10 Å/fs employing 0.6 mV/Å, which is similar to the terminal velocity for a bipolaron in standard armchair nanoribbons for the same electric-field strength.[23] Such similarities in saturation velocities between these two types of nanoribbons come from the equivalences of the charge localization profiles presented by them. The presence of bosons also leads to the tantalizing possibility of Bose−Einstein condensates (BECs) in this material. Possible BEC applications in graphene-based materials may involve, for example, quantum information processing (quantum computation), precision measurement by fabricating the most sensitive detectors using BECs, and the development of novel optical lattices that could be modified by varying the interplanar spacing.

AUTHOR INFORMATION

Corresponding Author

Luiz A. Ribeiro Junior − *Institute of Physics, University of Brasília, 70.919-970, Brazil;* orcid.org/0000-0001-7468-2946; Email: ribeirojr@unb.br

Authors

Marcelo L. Pereira Júnior − *Institute of Physics, University of Brasília, 70.919-970, Brazil*

Geraldo M. e Silva − *Institute of Physics, University of Brasília, 70.919-970, Brazil*

Complete contact information is available at: https://pubs.acs.org/10.1021/acs.jpclett.0c01489

Notes

The authors declare no competing financial interest.

ACKNOWLEDGMENTS

We gratefully acknowledge the financial support from Brazilian Research Councils CNPq, CAPES, and FAPDF and CENAPAD-SP for providing the computational facilities. L.A.R.J. gratefully acknowledges the financial support from FAP-DF grant 00193.0000248/2019-32. L.A.R.J. and G.M.e.S. gratefully acknowledge, respectively, the financial support from CNPq grants 302236/2018-0 and 304637/2018-1. M.L.P.J. acknowledges his colleague Gustavo Xavier Antunes Petronilo for valuable discussions.

REFERENCES

(1) Ostroverkhova, O. Organic Optoelectronic Materials: Mechanisms and Applications. *Chem. Rev.* **2016**, *116*, 13279−13412.

(2) Torsi, L.; Magliulo, M.; Manoli, K.; Palazzo, G. Organic field-effect transistor sensors: a tutorial review. *Chem. Soc. Rev.* **2013**, *42*, 8612−8628.

(3) Sekitani, T.; Nakajima, H.; Maeda, H.; Fukushima, T.; Aida, T.; Hata, K.; Someya, T. Stretchable active-matrix organic light-emitting diode display using printable elastic conductors. *Nat. Mater.* **2009**, *8*, 494−499.

(4) Kippelen, B.; Brédas, J.-L. Organic photovoltaics. *Energy Environ. Sci.* **2009**, *2*, 251−261.

(5) Zhang, Q.; Sun, Y.; Xu, W.; Zhu, D. Organic Thermoelectric Materials: Emerging Green Energy Materials Converting Heat to Electricity Directly and Efficiently. *Adv. Mater.* **2014**, *26*, 6829−6851.

(6) Geim, A. K.; Novoselov, K. S. The rise of graphene. *Nat. Mater.* **2007**, *6*, 183−191.

(7) Novoselov, K. S.; Geim, A. K.; Morozov, S. V.; Jiang, D.; Zhang, Y.; Dubonos, S. V.; Grigorieva, I. V.; Firsov, A. A. Electric Field Effect in Atomically Thin Carbon Films. *Science* **2004**, *306*, 666−669.

(8) Son, Y.-W.; Cohen, M. L.; Louie, S. G. Energy Gaps in Graphene Nanoribbons. *Phys. Rev. Lett.* **2006**, *97*, 216803.

(9) Han, M. Y.; Özyilmaz, B.; Zhang, Y.; Kim, P. Energy Band-Gap Engineering of Graphene Nanoribbons. *Phys. Rev. Lett.* **2007**, *98*, 206805.

(10) Son, Y.-W.; Cohen, M. L.; Louie, S. G. Half-metallic graphene nanoribbons. *Nature* **2006**, *444*, 347−349.

(11) Stafstrom, S. Electron localization and the transition from adiabatic to nonadiabatic charge transport in organic conductors. *Chem. Soc. Rev.* **2010**, *39*, 2484−2499.

(12) Heeger, A. J. Semiconducting polymers: the Third Generation. *Chem. Soc. Rev.* **2010**, *39*, 2354−2371.

(13) Schwab, M. G.; Narita, A.; Osella, S.; Hu, Y.; Maghsoumi, A.; Mavrinsky, A.; Pisula, W.; Castiglioni, C.; Tommasini, M.; Beljonne, D.; et al. Bottom-Up Synthesis of Necklace-Like Graphene Nanoribbons. *Chem. - Asian J.* **2015**, *10*, 2134−2138.

(14) Su, W. P.; Schrieffer, J. R.; Heeger, A. J. Solitons in Polyacetylene. *Phys. Rev. Lett.* **1979**, *42*, 1698−1701.

(15) Castro Neto, A. H.; Guinea, F.; Peres, N. M. R.; Novoselov, K. S.; Geim, A. K. The electronic properties of graphene. *Rev. Mod. Phys.* **2009**, *81*, 109−162.

(16) Heeger, A. J.; Kivelson, S.; Schrieffer, J. R.; Su, W. P. Solitons in conducting polymers. *Rev. Mod. Phys.* **1988**, *60*, 781−850.

(17) Ferreira da Cunha, W.; de Oliveira Neto, P. H.; Terai, A.; Magela e Silva, G. Dynamics of charge carriers on hexagonal nanoribbons with vacancy defects. *Phys. Rev. B: Condens. Matter Mater. Phys.* **2016**, *94*, 014301.

(18) de Oliveira Neto, P. H.; Teixeira, J. F.; da Cunha, W. F.; Gargano, R.; e Silva, G. M. Electron-Lattice Coupling in Armchair Graphene Nanoribbons. *J. Phys. Chem. Lett.* **2012**, *3*, 3039−3042.

(19) da Cunha, W. F.; Ribeiro, L. A.; de Almeida Fonseca, A. L.; Gargano, R.; e Silva, G. M. Impurity effects on polaron dynamics in graphene nanoribbons. *Carbon* **2015**, *91*, 171−177.

(20) Fischer, M. M.; Ribeiro Junior, L. A.; da Cunha, W. F.; de Sousa, L. E.; e Silva, G. M.; de Oliveira Neto, P. H. Ultrafast direct generation of quasiparticles in graphene nanoribbons. *Carbon* **2020**, *158*, 553−558.

(21) de Oliveira Neto, P. H.; Van Voorhis, T. Dynamics of charge quasiparticles generation in armchair graphene nanoribbons. *Carbon* **2018**, *132*, 352−358.

(22) Ribeiro, L. A.; da Cunha, W. F.; Fonseca, A. L. d. A.; e Silva, G. M.; Stafström, S. Transport of Polarons in Graphene Nanoribbons. *J. Phys. Chem. Lett.* **2015**, *6*, 510−514.

(23) Silva, G. G.; Ribeiro Junior, L. A.; Pereira Junior, M. L.; Fonseca, A. L. d. A.; de Sousa Júnior, R. T.; Silva, G. M. e. Bipolaron Dynamics in Graphene Nanoribbons. *Sci. Rep.* **2019**, *9*, 2909.

(24) Yang, H.; Mayne, A. J.; Boucherit, M.; Comtet, G.; Dujardin, G.; Kuk, Y. Quantum Interference Channeling at Graphene Edges. *Nano Lett.* **2010**, *10*, 943−947.

(25) Vos, F.; Aalberts, D.; van Saarloos, W. Simple method for calculating the speed of sound in tight-binding models: Application to the Su-Schrieffer-Heeger model. *Phys. Rev. B: Condens. Matter Mater. Phys.* **1996**, *53*, R5986−R5989.

(26) Silva, G. G.; da Cunha, W. F.; de Sousa Junior, R. T.; Almeida Fonseca, A. L.; Ribeiro Júnior, L. A.; e Silva, G. M. Influence of quasiparticle density over polaron mobility in armchair graphene nanoribbons. *Phys. Chem. Chem. Phys.* **2018**, *20*, 16712−16718.

https://dx.doi.org/10.1021/acs.jpclett.0c01489
J. Phys. Chem. Lett. 2020, 11, 5538−5543